KSME

Springer

Journal of Mechanical Science and Technology 36 (11) 2022

Original Article
DOI 10.1007/s12206-022-1026-5

Keywords:
· Additive manufacturing
· Compliant mechanism
· Constant velocity joint
· Universal joint

Correspondence to:
Raşit Karakuş
rasitkarakus@hacettepe.edu.tr

Citation:
Karakuş, R., Tanık, Ç. M. (2022). Compliant universal joint with preformed flexible segments. Journal of Mechanical Science and Technology 36 (11) (2022) 5639~5648.
http://doi.org/10.1007/s12206-022-1026-5

Received February 14th, 2022
Revised June 2nd, 2022
Accepted July 13th, 2022

† Recommended by Editor Hyun-Gyu Kim

Compliant universal joint with preformed flexible segments

Raşit Karakuş[1] and Çağıl Merve Tanık[2]

[1]Department of Mechanical Engineering, Hacettepe University, 06800 Ankara, Turkey, [2]Aselsan Inc., 06200 Ankara, Turkey

Abstract This paper introduces an original, fully compliant universal joint design. Many mechanisms with different dimensions are investigated. The proposed design is a single-piece compliant mechanism. The number of flexible segments is a design parameter determined as a function of transferred torque. The mechanism can be produced by additive manufacturing from polylactic acid and polypropylene. It is possible to produce the proposed design as a single piece of polypropylene by additive manufacturing and injection molding methods; thus, it has the advantage of ease in manufacturing. The proposed design's bending and torque transmission capacities are determined by applying analytical and numerical methods. Furthermore, a prototype was manufactured, and experiments were conducted. It is verified that the results of the experiments are consistent with theoretical approaches. The proposed fully compliant universal joint design has a great potential in the industry.

1. Introduction

Universal joints or power transmission couplings are spatial mechanisms used in general machinery to transfer rotary motion or energy between two inclined shafts. For a primary power transmission solution, Hooke's universal joint or Cardan joint has been used widely in the literature [1]. However, this coupling is not a constant velocity joint. As the misalignment angle between the two axes increases, the fluctuation of the transferred speed also increases accordingly. This fluctuation may cause a drastic increase in the stress acting on the members of the universal joint and vibrations on the driven shaft [2]. To overcome the non-uniformity of the rotational speeds of the shafts, different types of constant velocity universal joints (CV joints) have been proposed. In Refs. [3, 4] classification of the homokinetic couplings and their performance has been presented. There are different types of rigid constant velocity joints like Double Hooke, Rzeppa [5], Culver [6], Thompson [7], Kocabas [8], Yaghoubi and Sanaeifar [9] in the literature.

Compliant mechanisms gain some or all of their motion through the deflection of flexible members [10] and have lots of advantages such as low cost, reduced weight and number of parts, less noise, and no need for lubrication [11]. Besides, compliant mechanisms do not need springs to return the mechanism to its initial position because they store elastic energy when they deformed. One of the disadvantages is the analysis and design of compliant mechanisms that experience large and nonlinear deflections are difficult. The pseudo-rigid-body model (PRBM) is used to simplify the study of the compliant mechanisms [11]. Compliant mechanisms are classified as fully and partially compliant mechanisms [12]. There are several compliant universal joints [13], [14]. In Tanık and Parlaktaş's study, a compliant Cardan universal joint is proposed [15]. In the original design, two identical parts are assembled at right angles. Each of the identical parts can be produced from planar materials. Therefore, manufacturing of the proposed design is easy. In Tanık et al.'s paper, the first compliant Cardan universal joint made of steel is studied [16]. Machekposhti et al. proposed a large deflection compliant constant velocity universal joint [17]. PRBM and the kinematic of the mechanism are analyzed. Machekposhti et al. introduced a potentially monolithic, fully compliant CV joint in their study [18].

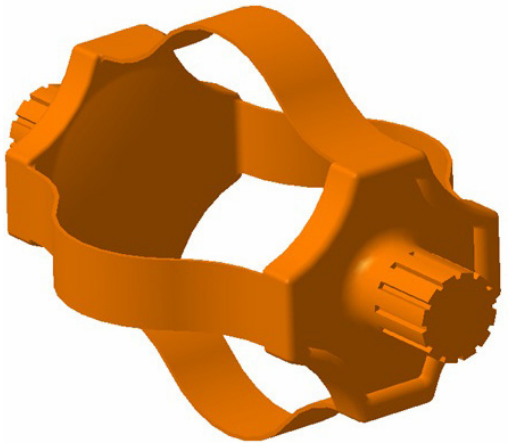

Fig. 1. The original compliant universal joint.

This paper introduces an original design for a fully compliant universal joint and describe the fundamentals of the proposed design. This monolithic and simple universal joint design has the advantage of ease in miniaturizing.

Two rigid segments on each side of the compliant universal joint are connected by predeformed flexible segments (Fig. 1). Rigid segments are used as input and output shafts, while flexible segments are deformed to obtain required shaft angles. Moreover, flexible segments transmit torque from the input to the output shaft.

The design of the compliant universal joints is discussed in the following sections. In Sec. 2, dimensions of the compliant universal joint with predeformed links are discussed, and the geometrical approach of the design is proposed. In Sec. 3, PRBM and deflection of the compliant segment are investigated. Secs. 4-6 stress analysis for only bending, torque, and combined loading cases are investigated analytically for initial design stages and verified with the finite element modeling. Three-dimensional plots are represented in Sec. 7 as design charts. The proposed design is then verified with the experimental setup in Sec. 8.

2. Dimensions of the fully compliant universal joint with predeformed flexible segments

Generally, it is advantageous to develop a design procedure for compliant mechanisms to obtain an analytic solution. In Fig. 2, undeformed and deformed (hatched) shapes of the proposed fully compliant universal joint are presented. The model shown in Fig. 2 is symmetric about its y-axis. $\mathrm{R_h}$ is the height of the universal joint, L is the horizontal distance between C_1 and C_3 points, β is the universal joint's bend angle with respect to x -axis. Each flexible segment of the compliant universal joint consists of four equivalent arcs that are denoted by C_1C_2, C_2C_3 and their symmetry about the y -axis. The main criterion for determining the radius and the length of each arc is the summation of the lengths of the identical arcs should

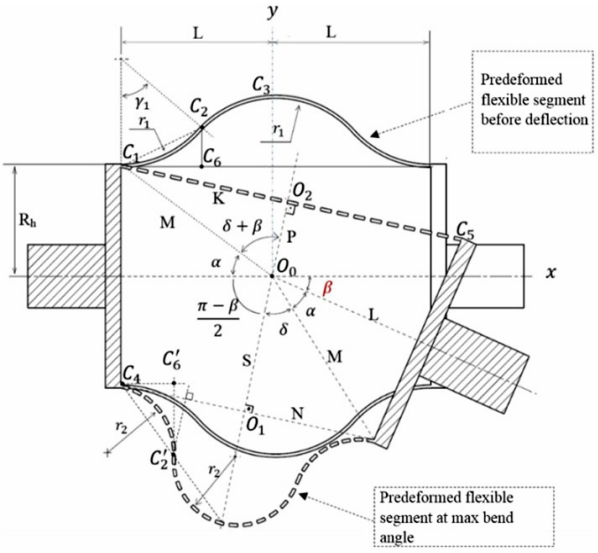

Fig. 2. Compliant universal joint at undeformed and deformed positions.

be equal to the length of the flexible segment (C_1C_5) at maximum bend angle (β_{max}).

For the stretched position of the compliant universal joint, Eq. (5) is obtained using geometric identities (Eqs. (1)-(4)) and defines the relationship between the radius of each arc (r_1) and its arc angle (γ_1), where 2K is the length of the flexible segment at β_{max} . Note that, in order to simplify the analytical model, the deformed position of the flexible segments is assumed to be perfectly circular.

$$\tan\alpha = \frac{\mathrm{R_h}}{\mathrm{L}} \tag{1}$$

$$\alpha + \delta = \frac{\pi - \beta}{2} \tag{2}$$

$$\mathrm{M} = \sqrt{\mathrm{L}^2 + \mathrm{R_h}^2} \tag{3}$$

$$\mathrm{N} = \mathrm{M}\sin\delta \tag{4}$$

$$r_1\gamma_1 = \frac{\mathrm{K}}{2} = l \tag{5}$$

According to the $C_1C_2C_6$ triangle in Fig. 2, r_1 is defined as a function of γ_1 and L as presented in Eq. (6).

$$r_1 = \sqrt{\frac{\mathrm{L}^2}{8}\frac{1}{(1-\cos\gamma_1)\cos\frac{\gamma_1}{2}^2}} \tag{6}$$

Eqs. (5) and (6) are solved simultaneously by numerical methods. Each value of r_1, γ_1 is calculated by using Eq. (5). Iterations can be done until Eq. (6) is satisfied for a specific r_1, γ_1 value. Since L, $\mathrm{R_h}$, and β are defined as design parameters, there is a unique solution for r_1, γ_1 that can be derived iteratively. Using these parameters, a new compliant universal joint can be designed.

3. Angular deflection analysis of predeformed flexible segments

The deflection of the flexible segments is a function of the bend angle (β) in the proposed design. During the bending, each of the initially curved flexible segments acts like a fixed-guided beam. The fixed-guided beam theories and initially curved beam theories are combined by separating the flexible segments into four equivalent pieces. Separation points are the neutral axis of the flexible segments where stress is zero in its longitudinal axis (i.e. C_2 in Fig. 2). As a result, each part can be investigated as an initially curved beam that undergoes large deflection. For a deflection resulting from a certain bend angle, the endpoint of the half segment (C_2 Fig. 3) will be translated to its new position ($C_2^{'}$ Fig. 3). When the amount of deflection is determined by employing the end coordinates of the half segment, the amount of stress can be determined by using the theories that are developed for initially curved cantilever beams. The difference between the initial and final positions of the endpoint gives the amount of deformation $(\theta_f - \theta_i)$ that the half segment undergoes (Fig. 3). The amount of deflection (θ_f) is determined by geometrical analysis using the PRBM presented in Fig. 3.

Eq. (7) is defined as a function of β and simplified to Eq. (8). After θ_f is determined by using a half tangent formula.

$$-\left(\frac{\rho l\frac{\sin\beta}{2}\cos\beta}{2}\right)\sin\theta_f+\rho l\left(\frac{\sin\beta^2}{2}-1\right)\cos\theta_f+\left(\sin\frac{\beta}{2^2}-1\right)+\frac{\mathrm{N}}{2}\cos\beta/2=0 \tag{7}$$

$$A\sin\theta_f+B\cos\theta_f+C=0 \tag{8}$$

where,

$$A=-\frac{\rho l}{2}\sin\beta$$

$$B=-\rho l\cos^2\beta/2$$

$$C=\frac{N}{2}\cos\beta/2-l(1-\rho)\cos^2\beta/2$$

where l is equal to the arc length of the quarter portion of the flexible segment in Eq. (5).

Since the length of the flexible segment is determined, one can determine the end coordinates of the beam as a function of the initial and final angles of PRBM (Fig. 3).

$$a_i=\frac{l\left(1-\rho\left(1-\cos\theta_i\right)\right)}{2} \tag{9}$$

$$b_i=\rho l\sin\theta_i \tag{10}$$

$$a_f=\frac{l\left(1-\rho\left(1-\cos\theta_f\right)\right)}{2} \tag{11}$$

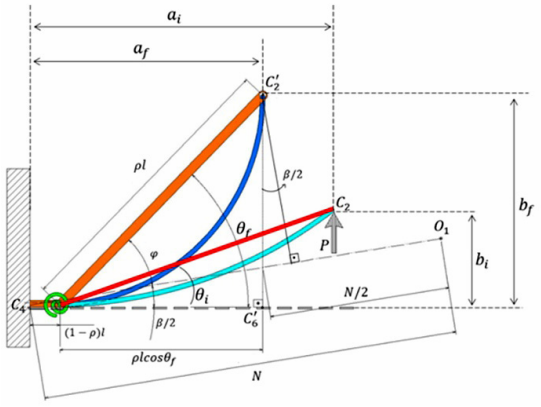

Fig. 3. Deflected and undeflected positions of the compliant segment and its PRBM.

$$b_f=\rho l\sin\theta_f. \tag{12}$$

4. Static analysis for bending-only case

To determine the bending capacity of the proposed design, static analysis for the bending-only case was investigated. Numerical and analytical analyses were conducted for the universal joint whose shafts intersect at a bend angle β. The maximum normal stress at the compliant segments was calculated for different bend angle values.

Generally, in compliant mechanisms bending is the predominant type of deflection and in the proposed design primary source of this deflection is the “beam end moment” type of loading, both small and large deflections [11, 15]. The relationship between the moment and slope of the deflected beam at its end is given in Eq. (13).

$$M_s=K_s\left(\Delta\theta\right)_{deg} \tag{13}$$

where K_s is the spring constant which is defined in Eq. (14).

$$K_s=\rho K_\theta EI/l \tag{14}$$

where ρ is a function of characteristic radius factor γ.

The maximum stress for this type of loading is [11]:

$$\sigma_{bending}=M_s t_h/2I_1 \tag{15}$$

where $I_1=wt_h^3/12$.

For the numerical analysis, ANSYS® is used, and the beam is modelled as fixed support to one end of the design, and the other end is bent by remote displacement to rotate the output shaft at the desired bend angle. For the bend angles smaller than 10°, small deflection analysis is selected [19]. Large deflection analysis is chosen for the larger bend angles. The equivalent stress values for the compliant links are obtained for varying number of arms, width, and thickness values. In Fig. 4,

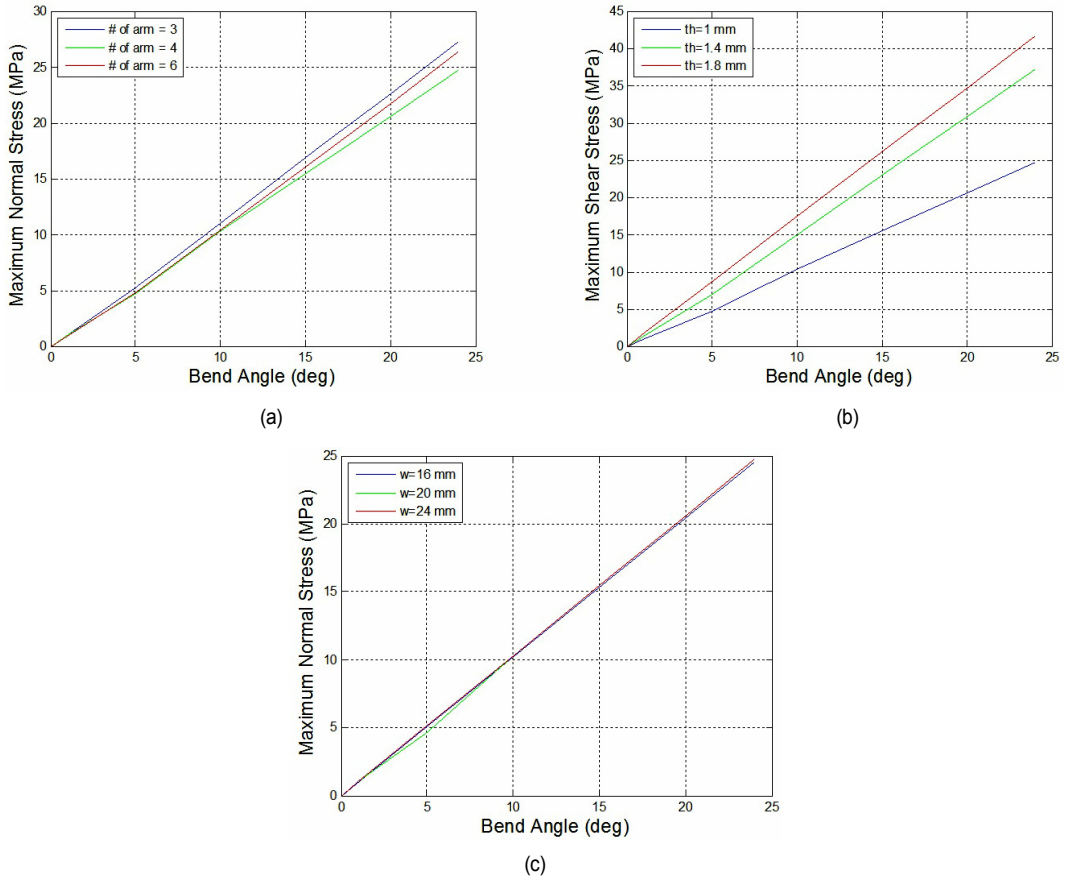

Fig. 4. Bend angle vs. maximum normal stress values for (a) constant w and t_h, varying number of arms; (b) constant w and number of arms, varying t_h; (c) constant t_h and number of arms, varying w.

the effect of the number of arms on bending capacity is plotted while keeping the width and thickness values constant at 20 mm and 1 mm, respectively. Maximum stress values are very close to each other for 3, 4, and 6 arms for the same amount of bend angles (Fig. 4(a)).

For the same amount of deflection, the beam with a larger thickness is subjected to larger stress [11]. Therefore, the maximum stress increases as the thickness increases. As expected, the thicker flexible segments provide higher torque capacity in applications up to 10° bend angle.

To determine the effect of the width, the thickness and the number of arms are kept constant, and the width of the compliant segments is varied. The parameters are chosen as the number of arm = 4, t_h = 1 mm, and w = 16, 20, and 24 mm. The results are presented in Fig. 4(c). It is observed that the width of the flexible segment does not affect the bending capacity. According to Fig. 2, there is no stress variation along the z-axis on the cross-section at C_1. However, stress is varied in the y-axis.

5. Static analysis for the torque-only case at zero bend angle

In this part of the simulations, one end of the mechanism is fixed while the other is subjected to the specified torque. After simulations are conducted, maximum shear stress values corresponding to output torque for zero bend angle are obtained. The applied torque is increased to obtain maximum shear stress values. In the simulations, width and number of arm, values are kept constant at 20 mm and 4, respectively. Simulations are performed for three different flexible segment thicknesses. There is a linear relationship between maximum shear

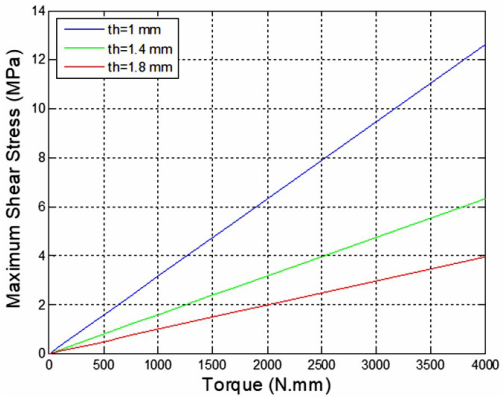

Fig. 5. Torque vs. maximum shear stress values for fixed w and number of arms, varying t_h without bending.

stress and output torque, as presented in Fig. 5. Larger torque transmitting capacity is obtained with thicker flexible segments when there is no bending. Decreasing the cross-sectional area of the flexible segment results in a decrease in the transmitted torque. Therefore, if the width of the segment decreases, maximum shear stress increases. Note that the number of arms can be increased to reduce the maximum shear stress.

6. Static analysis for both bending and output torque case

In this part of the study, static torque transmission capacities of the compliant universal joint for different flexible segment thicknesses, widths, and the number of arms corresponding to different bend angles were investigated analytically and numerically. The torque can be applied as forces of identical magnitude acting at the end of each quarter portion of the flexible segments on the universal joint that are equally positioned from the geometrical center of the joint. Each of these forces (F) can be determined by using Eq. (16). The proposed design has four flexible segments; therefore input torque is divided by 4. According to the number of arms, the denominator of Eq. (16) will be changed.

$$F = T_{input} / 4\left(h_{body} + b\right). \tag{16}$$

This force (F) causes both bending moment (M_a) and torque (T_b) at the fixed end of the quarter portion of the flexible segment, as presented in Fig. 1. The normal stress due to the bending moment (M_a) can be calculated by using Eq. (17) where $I_2 = t_h w^3 / 12$.

$$\sigma_{M_a} = F a_f w / 2 I_2 \tag{17}$$

The shear force due to the torque (T_b) is calculated by using Eq. (18) where α = 0.33 for the rectangular cross-sections with $w / t_h = \infty$ [20].

$$\tau_{T_b} = F b_f / \alpha w \left(t_h\right)^2. \tag{18}$$

Once the normal and shear stresses at points 1 and 2 are determined (Fig. 1), the equivalent stress can be calculated according to the von Mises yield criterion:

$$\sigma_{von\ Mises1,2} = \sqrt{\frac{\left(2\sigma_{bending} \pm \sigma_{M_a}\right)^2 + 6\tau_{T_b}^2}{2}} \tag{19}$$

Eqs. (16)-(19) are used to determine the initial dimensions of the proposed universal joint. The obtained model is then analyzed by the finite element method for verifying the results.

The finite element analysis is performed in three steps: In the first step, the obtained results using the analytical model are verified by finite element analysis. Since the stress values are relatively low, the differences between numerical and analytical values are compared instead of percentage error. It is determined that the maximum deviation between the two methods is less than 3 MPa, which is close enough for the initial design of the joint. In the second step, one end of the compliant universal joint is bent while keeping the other end fixed. Finally, the bent shaft is subjected to torque in the third step. Since the deflections of the flexible segments are large, a nonlinear solution is applied in the simulations. Torque values are applied iteratively up to the yield limit of the material to determine the maximum torque that the universal joint can transmit onset of yielding.

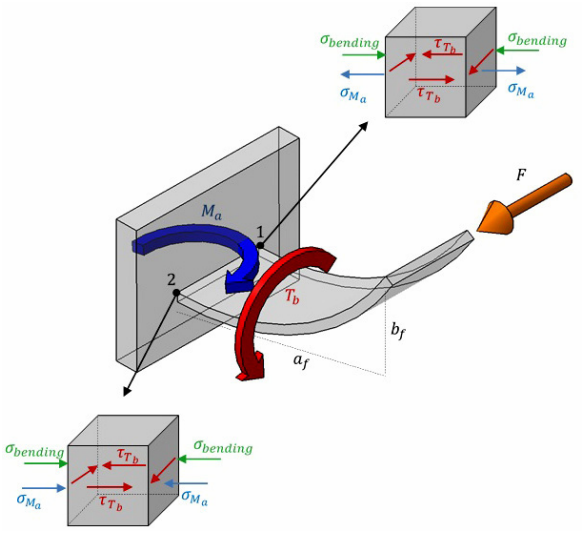

Fig. 6. Quarter portion of the flexible segment and infinitesimal cubes of the critical points 1 and 2.

To investigate the effect of the flexible segment thickness, varying thickness values are used while the width and the number of arms are kept constant. The results are presented in Fig. 2(b) for the parameters w = 20 mm, number of arms = 4, and t_h = 1, 1.4, and 1.8 mm.

It is observed that the torque capacity increases as the thickness of the flexible segments increases. However, increasing the thickness results in a decrease in the maximum bend angle capacity. According to the mechanical properties of the polypropylene [21] for t_h = 1 mm, the maximum bend angle is 21.4° onset of yielding, and the maximum torque capacity is 802 N.mm when there is no bending. For t_h = 1.8 mm, these values are 12.6° and 2396 N.mm, respectively. Therefore, as in most compliant mechanisms, the primary design parameter that defines the torque and bending capacity is the thickness of the flexible segments. Results are presented in Fig. 2(c) that the optimum thickness value can be obtained.

7. Design plots for the compliant universal joint

It can be observed from Fig. 8 that as the flexible segment thickness increases, the torque capacity also increases while decreasing the maximum bend angle capacity of the mechanism. For the mechanism with t_h = 1 mm, the maximum bend

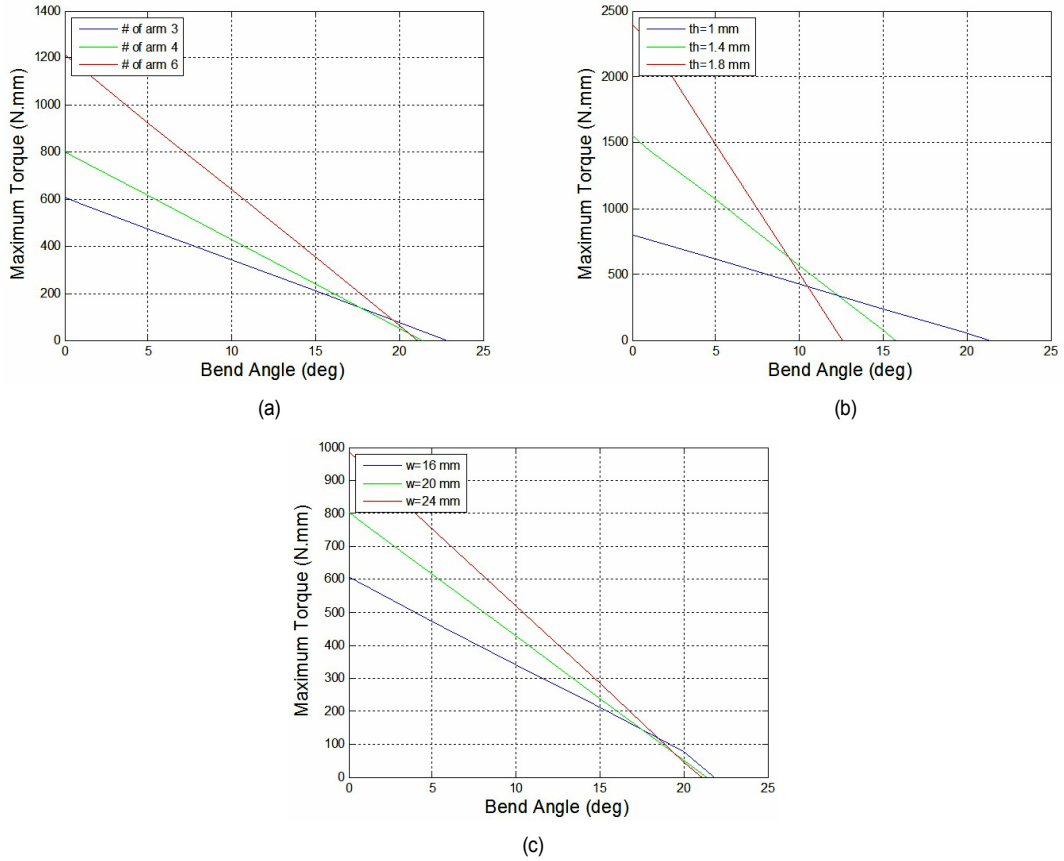

Fig. 7. Bend angle vs. maximum torque stress values for (a) fixed w and t_h, varying number of arms; (b) fixed w and number of arms, varying t_h; (c) fixed t_h and number of arms, varying w.

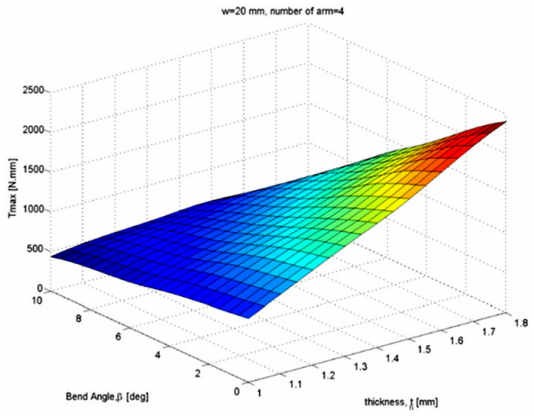

Fig. 8. Maximum torque values for w = 20 mm, number of arms = 4.

angle reaches 20° before yielding, and its maximum torque capacity is about 800 N.mm when the bend angle is zero. For the mechanism with t_h = 1.8 mm, these values are 10.8° and 2500 N.mm. This situation indicates that the thickness of flexible segments of the compliant universal joint is a major design parameter that defines its torque and bending capacity.

Further simulations were performed to determine the effect of the number of arm flexible segments of the compliant universal joint for varying bend angles while keeping the thickness and width constant. The parameters are the number of arms = 3, 4, and 6 and t_h = 1 mm. The simulation results are presented in Fig. 8. Let's consider the mechanism's performance with a thickness of 1 mm and width of 20 mm in Fig. 9. When the bend angle exceeds 15°, the torque capacity is the same for three, four, and six flexible segments. However, when the bend angle is 1°, the torque capacity of the universal joint with six flexible segments is 99 % more than the universal joint with three flexible segments. Note that there is a linear relationship between the number of arms and torque capacity at lower bend angles. Therefore, the design with four arms has a torque capacity of 33 % more than the design with three arms.

To observe the effect of the width, the width of the flexible segment is varied while keeping the number of arms and thickness constant. The parameters are t_h = 1 mm, and the number of arms = 4. The results are presented in Fig. 10. It is observed that the width of the flexible segment has a minor effect on the torque capacity when the bend angle is high. However, the torque capacity increases considerably as the width increases for smaller bend angles. For example, let's consider the mechanism's performance with a flexible segment thickness of 1 mm in Fig. 10. When the bend angle is 1°, the torque capacity of the flexible segment with the highest width (w = 24 mm) is 54 % more than the lowest one (w = 16 mm).

A general result is obtained from all of the analyses and

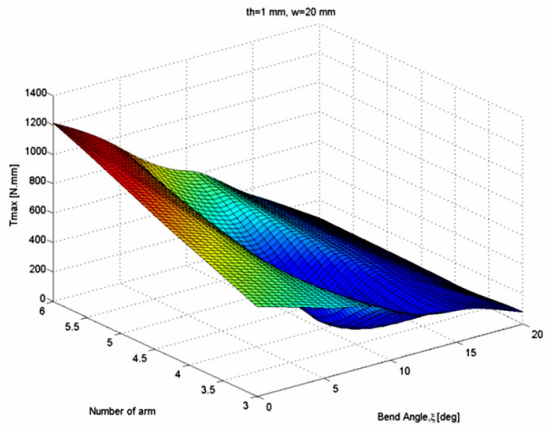

Fig. 9. Maximum torque values for w = 20 mm, t_h = 1 mm.

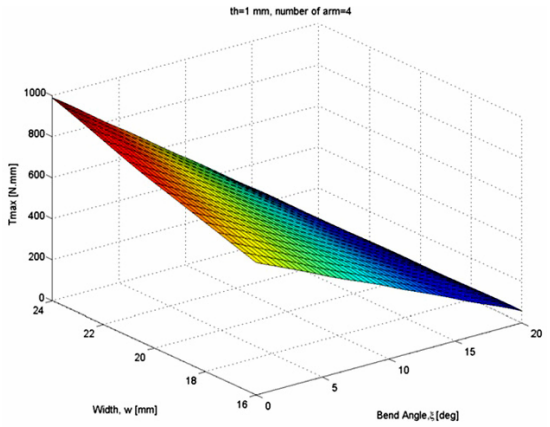

Fig. 10. Maximum torque values for t_h = 1 mm, number of arms = 4.

simulations: For large bend angles, the bending moment of the flexible segment increases; thus bending stress for the thicker segments becomes more dominant and their torque capacity decreases. Intersections of the curves (Figs. 8-10) can be used as a design criterion to decide the dimensions of the compliant universal joint according to the requirements of the application.

8. FEA of flexible hinges at out of plane

The analytical model was used for the initial design of the proposed joint. The detailed analysis of the flexible hinges was performed by FEA. The analytical model is based on 2D analysis. However, during the joint's rotational motion, the flexible hinges move through the out of plane. The flexible hinges perform a spatial motion that is a function of the bend angle during the rotational motion. The initial model was analyzed at the out-of-plane position of the flexible hinges.

The FEA of the flexible hinge at 90° is presented in Fig. 11. For the given parameters, the maximum stress due to the bending is determined as 25 MPa at β = 24°, which is lower than the yield point of the polypropylene. Furthermore, 200 N.mm torque is applied to input shaft at maximum bend

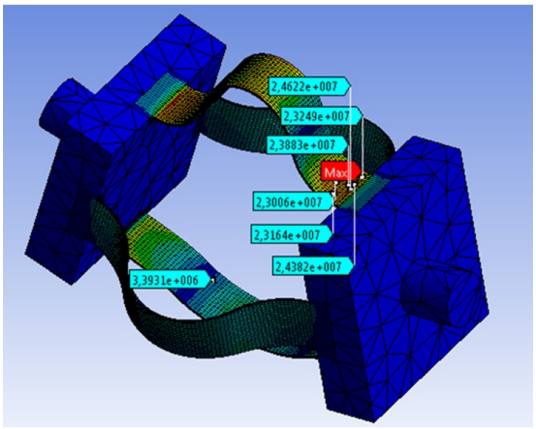

Fig. 11. FEA of the flexible hinge at 90º with the parameters of w = 20 mm, t_h = 1 mm, R_h = 70 mm and L = 100 mm.

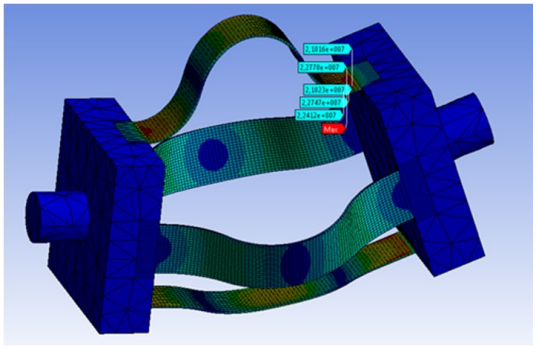

Fig. 12. FEA of the flexible hinge at 90º with 200 N.mm torque.

angle for the same parameters. Maximum stress was determined as 28 MPa for this case, which is still lower than the yield limit of the polypropylene (Fig. 12).

9. Experimental analysis

To verify theoretical calculations, we built an experimental setup. The experimental setup with four flexible segments was manufactured according to the given design parameters. Let the dimensions of the flexible segments be w = 20 mm, t_h = 1 mm, R_h = 70 mm and L = 100 mm.

Using the Eqs. (1)-(5), N & and l are determined. The bend angle (β) of the compliant universal joint is a design parameter. Substituting N = 41.63, l = 28.1 mm, $\beta/2$ = 12°, ρ = 0.83.

θ_f is determined by Eq. (8) where A = -4.74, B = -22.31, C = 15.79.

$$\begin{aligned} &t^2 - 0.25t - 0.17 = 0 \\ &t_1 = 0.556 \,\&\, t_2 = -0.308 \\ &\theta_{f1} = 58.19° \,\&\, \theta_{f2} = -36.32° \end{aligned} \tag{20}$$

The maximum stress at β = 24° is determined as $\sigma_{bending}$ =

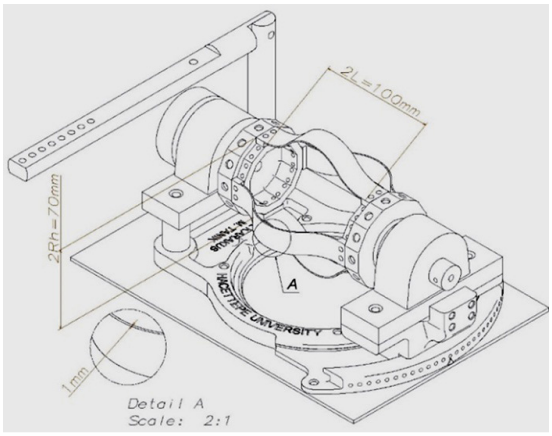

Fig. 13. Technical drawing of the experimental setup.

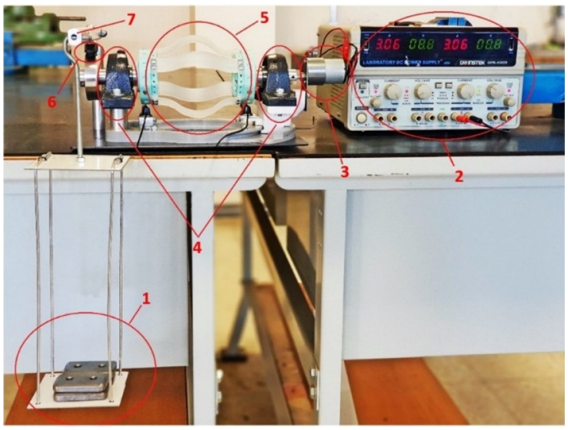

Fig. 14. Experimental setup.

28, 19 MPa (Eq. (15)).

The resulting stress is lower than the yield strength of the PP. This condition is only valid if the proposed joint is manufactured with PP sheet material. Since the experimental setup was designed to be produced by additive manufacturing techniques, the mechanical properties of PP filament were used. The yield strength of the PP filament is 19 MPa [21], which is lower than the PP sheet.

The proposed compliant universal joint design consists of two rigid bodies at each end and flexible segments between these rigid bodies. The design is produced by the additive manufacturing method. Also, there are several experimental compliant mechanism setups in the Refs. [22, 23]. A compliant universal joint is designed as an assembly to perform experiments using different flexible segment dimensions and numbers (Fig. 13). However, it is possible to produce the compliant universal joint as a single piece of PP material by both additive manufacturing and injection molding methods. Rigid and compliant parts are made from polylactic acid (PLA) and PP, respectively.

Experimental analyses were conducted by using the setup shown in Fig. 11. The experimental setup consists of seven main parts: A weight (1) is attached to the braking lever (7) that is used for applying constant braking force on the braking pad (6). Power supply (2) is used for DC electric motor (3), creating input torque. The proposed compliant universal joint (5) with four flexible segments is assembled between two ball bearings (4).

The torque and the bending capacity were observed to verify the analytical and numerical results. Furthermore, it should be verified that the proposed universal joint is suitable for additive manufacturing methods. Finally, the speed variation between input and output shafts was compared.

Before the experiment, the output torque was determined as a function of the weight (1) hanging on the braking lever in Fig. 14. For a certain amount of mass, the force required to rotate the output shaft is measured by a force gauge. The input and the output shafts are disconnected for the output torque measurement. As a result, the output torque characteristics of the test setup are determined as a function of hanging mass.

The test procedure was started with zero output torque, and the compliant universal joint was operated at different bend angles. We observed that the designed universal joint and the test setup were in good agreement by means of the bending capacity. The smoothness of the motion is also an important parameter for mechanisms. The smoothness of the proposed joint under working conditions was tested by measuring the variation of current drawn by the input motor. Since the refresh rate of the power supply while displaying the current was insufficient, an oscilloscope was integrated into the experimental setup. The drawn current by the input motor at different bend angles is read from the oscilloscope graphically at 20 Hz. The current variation was measured less than 7 % indicates the input motor does not need to apply greater torques at different angular positions.

The average maximum output torque was 1100 N.mm according to the analytical and numerical calculations. It was observed that the universal joint transmits the output torque up to 1000 N.mm at β = 0°; however, it failed at 1150 N.mm output torque.

The experimental results of the compliant universal joint at different bend angles are presented in Fig. 15. The experimental output torque limits agree with theoretical output torque limits. The slight differences between the theoretical and experimental results are mainly caused by manufacturing tolerances, thermal variations, and uncontrollable friction losses. It should be remembered that PP filament has lower yield strength than PP sheet. For this reason, the maximum bend angle is limited to 20° (Fig. 15).

Another significant result derived from the experimental setup is that the additive manufacturing methods can be used for the compliant mechanisms. Since the directions of the layers may take an important place for the strength of the flexible segments, special attention is needed at the design stages [24, 25].

The rotational speed of the input-output shafts was also measured during operation at different bend angles. The input shaft of the compliant universal joint is connected to the drive

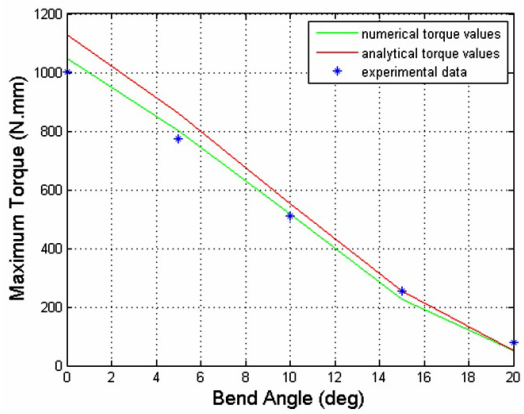

Fig. 15. Output torque variations with respect to bend angle.

motor and driven at various speeds. The output shaft is free to rotate. To observe the input-output shaft velocities, six magnets are attached around each of the shafts. The velocity data is read by using speedometers. Experimentally observed that the proposed design is a constant velocity joint for different bend angles.

10. Conclusions

This study proposes a novel compliant universal joint with predeformed flexible segments. To the best of our knowledge, this type of compliant universal joint is not studied in the literature. This design has advantages over other universal joint designs. It can be adapted easily by changing the width, thickness, and number of flexible segments according to the required bend angles and output torque values. The prototype is manufactured by the additive manufacturing method from PP. Moreover, the design is also suitable for plastic injection molding. Thanks to the scalability of compliant mechanisms, the compliant universal joint can be produced in a very wide dimensional range.

This study can be divided into five main steps. First, a parametric design procedure is proposed for the compliant universal joint. As a result, an adaptable universal joint design is presented. After this step, an analytical stress analysis is applied to the design. Since there is no solution method for initially curved fixed-guided beams in the literature, an alternative method for stress analysis is proposed. The proposed analytical method for stress analysis was verified using FEA. Many mechanisms with different flexible segment dimensions were analyzed. For the bending-only case, it is observed that the beam with a larger thickness is subjected to more considerable stress for the same amount of deflection. Therefore, maximum stress increases as the thickness increases. To realize the characteristics of the compliant universal joint, the maximum torque capacity of the mechanism was analyzed for zero bend angle. It is observed that if there is no bending, torque capacity has a linear relationship with the thickness of the flexible segment. In universal joint applications combined loading case, where both bending and output torque are applied, is the most common operational condition. Therefore, a combined loading case was examined to obtain the performance of the proposed design.

The width of the flexible segment has a minor effect in the bending-only case. However, for the combined loading case, it becomes one of the significant parameters that limit the torque capacity of the joint. For different combinations of the width, thickness, and the number of flexible segments, design charts are obtained as 3D graphics. Any designer who intends to use the proposed design can easily determine the required parameters using these 3D design plots.

From the experimental setup, we observed that the proposed compliant universal joint has constant velocity characteristics, which are very valuable.

From design stages to experimental setup, it is proved that the proposed compliant universal joint is capable of being used in many different areas.

References

[1] F. Schmelz, C. H. Seherr-Thoss and E. Aucktor, Universal jointed driveshafts for transmitting rotational movements, *In Universal Joints and Driveshafts*, Springer (1992) 1-28.

[2] C. H. Chiang, *Kinematics of Spherical Mechanisms*, United Kingdom: Cambridge University Press (1988).

[3] D. F. Machekposhti, N. Tolou and J. L. Herder, A review on compliant joints and rigid-body constant velocity universal joints towards the design of compliant homokinetic couplings, *J. of Mechanical Design,* 137 (3) (2015) 032301.

[4] D. F. Machekposhti, N. Tolou and J. L. Herder, The scope for a compliant homokinetic coupling based on review of compliant joints and rigid-body constant velocity universal joints, *Proceeding ASME IDETC/CIE 36th Mechanisms and Robotics Conference*, Chicago, 45035 (2012) 379-392.

[5] A. H. Rzeppa, *Constant Velocity Universal Joint*, United State Patent, 1665280 (1928).

[6] I. H. Culver, *Constant Velocity Universal Joint*, United States Patent, 3477249 (1969) 51.

[7] G. A. Thompson, *Constant Velocity Coupling and Control System Therefor*, United States Patent*,* 7144326 (2006).

[8] H. Kocabas, Deisgn and analysis of a spherical constant velocity coupling mechanism, *J. of Mechanical Design,* 129 (2007) 991-998.

[9] M. Yaghoubi and A. Sanaeifar, Design, manufacture and evaluation of a new flexible constant velocity mechanism for transmission of power between parallel shafts, *Journal of Mechanical Science and Technology,* 29 (2015) 3357-3361.

[10] L. L. Howell and A. Midha, A method for the design of compliant mechnaisms with small length flexural pivots, *ASME J. of Mechnaical Design,* 1 (116) (1994) 280-290.

[11] L. L. Howell, *Compliant Mechanisms*, New York: John Wiley & Sons, Inc. (2001).

[12] A. Midha, T. W. Norton and L. L. Howell, On the nomenclature, classification and abstractions of compliant mechanisms, *ASME*

J. of Mechanical Design, 1 (116) (1994) 270-279.
[13] B. Trease, Y. Moon and S. Kota, Design of large-displacement joints, *ASME J. of Mechanical Design,* 127 (2005) 788-798.
[14] L. Rubbert, S. Caro, J. Gangloff and P. Renaud, Using singulariities of parallel manipulators to enhance the rigid-body replacement, *ASME J. of Mechanical Design,* 136 (2014) 051010.
[15] E. Tanık and V. Parlaktaş, Compliant cardan universal joint, *J. of Mechanical Design*, 134 (2012) 021011.
[16] Ç. M. Tanık, V. Parlaktaş, E. Tanık and S. Kadıoğlu, Steel compliant cardan universal joint, *Mechanism and Machine Theory*, 92 (2015) 171-183.
[17] D. F. Machekposhti, N. tolou and J. L. Herder, A fully compliat constant velocity universal joint, *International Design Engineering Technical Conference & Computers and Information in Engineering Conference*, Boston, Massachusetts, 57120 (2015) V05AT08A014.
[18] D. F. Machekposhti, N. tolou and J. L. Herder, A fully compliant homokinetic coupling, *ASME J. of Mechanical Design,* 140 (1) (2018) 012301.
[19] V. Parlaktaş and E. Tanık, Single piece compliant spatial slider-crank mechanism, *Mechanism and Machine Theory,* 81 (2014) 1-10.
[20] R. G. Budynas and J. K. Nisbett, *Shigley's Mechanical Engineering Design*, New York: McGraw-Hill Education (2015).
[21] BASF, *Technical Data Sheet for Ultrafuse PP Version: 3.2* (2019).
[22] M. Garcia, K. McFall and A. Tekes, Trajectory control of planar closed chain, *Journal of Mechanical Science and Technology,* 35 (4) (2021) 1711-1719.
[23] A. Tekes, H. Lin and K. McFall, Design, modelling and experimentation of a novel compliant translational dwell mechanism, *Journal of Mechanical Science and Technology,* 33 (7) (2019) 3137-3145.
[24] V. Vega, J. Clements, T. Lam, A. Abad, B. Fritz, N. Ula and O. S. Es-Said, The effect of layer orientation on the mechanical properties and microstructure of a polymer, *J. of Materials Engineering and Performance,* 20 (6) (2011) 978-988.
[25] V. Kovan, G. Altan and E. S. Topal, Effect of layer thickness and print orientation on strength of 3D printed and adhesively bonded single lap joints, *J. of Mechanical Science and Technology,* 31 (5) (2016) 2197-2201.

Appendix. Supplementary data

https://www.youtube.com/watch?v=jRGxo9E9lpE

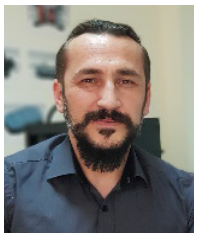

Raşit Karakuş works as a teaching assistant at Hacettepe University. He received his Ph.D. in Mechanical Engineering from Hacettepe University. His research interests include compliant mechanisms and electric vehicles.

Çağıl Merve Tanık works as an engineer in the Academic Relations Department at ASELSAN Academy. She received her Ph.D. in Mechanical Engineering from Middle East Technical University. Her research interests include compliant mechanisms and solid mechanics.